LETTERS

Emergence of the persistent spin helix in semiconductor quantum wells

J. D. Koralek[1], C. P. Weber[1,2], J. Orenstein[1,3], B. A. Bernevig[4], Shou-Cheng Zhang[5], S. Mack[6] & D. D. Awschalom[6]

According to Noether's theorem[1], for every symmetry in nature there is a corresponding conservation law. For example, invariance with respect to spatial translation corresponds to conservation of momentum. In another well-known example, invariance with respect to rotation of the electron's spin, or SU(2) symmetry, leads to conservation of spin polarization. For electrons in a solid, this symmetry is ordinarily broken by spin–orbit coupling, allowing spin angular momentum to flow to orbital angular momentum. However, it has recently been predicted that SU(2) can be achieved in a two-dimensional electron gas, despite the presence of spin–orbit coupling[2]. The corresponding conserved quantities include the amplitude and phase of a helical spin density wave termed the 'persistent spin helix'[2]. SU(2) is realized, in principle, when the strengths of two dominant spin–orbit interactions, the Rashba[3] (strength parameterized by α) and linear Dresselhaus[4] (β_1) interactions, are equal. This symmetry is predicted to be robust against all forms of spin-independent scattering, including electron–electron interactions, but is broken by the cubic Dresselhaus term (β_3) and spin-dependent scattering. When these terms are negligible, the distance over which spin information can propagate is predicted to diverge as α approaches β_1. Here we report experimental observation of the emergence of the persistent spin helix in GaAs quantum wells by independently tuning α and β_1. Using transient spin-grating spectroscopy[5], we find a spin-lifetime enhancement of two orders of magnitude near the symmetry point. Excellent quantitative agreement with theory across a wide range of sample parameters allows us to obtain an absolute measure of all relevant spin–orbit terms, identifying β_3 as the main SU(2)-violating term in our samples. The tunable suppression of spin relaxation demonstrated in this work is well suited for application to spintronics[6,7].

Transient spin-grating spectroscopy (TSG) is a powerful tool for searching for the persistent spin helix (PSH) because it enables measurement of the lifetime of spin polarization waves as a function of wavevector, **q**. In TSG, spin polarization waves of well-defined **q** are generated by exciting a two-dimensional electron gas (2DEG) with two non-collinear beams of light from a femtosecond laser. When the two incident pulses of light are linearly polarized in orthogonal directions, interference generates stripes of alternating photon helicity in the sample. Because of the optical orientation[8] effect in III–V semiconductors, the photon helicity wave generates a spin polarization wave in the 2DEG. The wavevector is varied by changing the angle between the interfering beams. The spin wave imprinted in the 2DEG acts as an optical diffraction grating, allowing its subsequent temporal evolution to be monitored by the diffraction of a time-delayed probe pulse[9].

In Fig. 1a we show a set of TSG decay curves for a 2DEG in an asymmetrically modulation-doped GaAs quantum well, which is expected to have both Rashba and Dresselhaus spin–orbit interactions. Each curve represents the decay of a spin grating at a specific **q**. The decay at $q \equiv |\mathbf{q}| = 0$ (not shown), measured by time-resolved Faraday rotation[10], follows a single exponential over nearly three orders of magnitude. With increasing **q**, the decay evolves towards the sum of two exponentials with nearly equal weights but very different rate constants. We fit the TSG decay curves with double exponentials and plot the resulting spin lifetimes in Fig. 1b, immediately observing very unusual spin-diffusion properties. The rapidly decaying component of

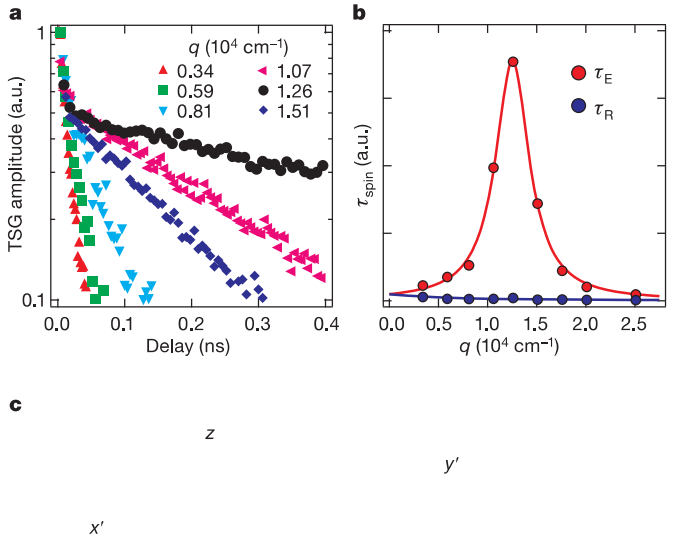

Figure 1 | Double-exponential decay of transient spin gratings. a, TSG decay curves at various wavevectors, **q**, for an asymmetrically doped 2DEG with a mixture of Rashba and Dresselhaus spin–orbit couplings. a.u., arbitrary units. **b**, Lifetimes for the spin–orbit-enhanced (τ_E) and -reduced (τ_R) helix modes extracted from double-exponential fits to the data in **a**. The solid lines are a theoretical fit (see text) using a single set of spin–orbit parameters for both helix modes. Error bars (s.d.) are the size of the data points. **c**, Illustration of a helical spin wave, which is one of the normal modes of the spin–orbit coupled 2DEG. In this picture, z is the growth direction [001], and the axes x' and y' respectively refer to the [11] and [1$\bar{1}$] directions in the plane of the 2DEG. The green spheres represent electrons whose spin directions are given by the arrows.

[1]Materials Science Division, Lawrence Berkeley National Laboratory, Berkeley, California 94720, USA. [2]Department of Physics, Santa Clara University, Santa Clara, California 95053, USA. [3]Department of Physics, University of California, Berkeley, California 94720, USA. [4]Princeton Center for Theoretical Science, Princeton University, Princeton, New Jersey 08540, USA. [5]Department of Physics, Stanford University, Stanford, California 94305, USA. [6]Center for Spintronics and Quantum Computation, University of California, Santa Barbara, California 93106, USA.

the TSG (lifetime, τ_R) displays ordinary diffusion in the sense that the spin lifetime is peaked at $q = 0$. On the other hand, the lifetime of the slowly decaying component (τ_E), is peaked sharply at a non-zero value of q.

The salient features of Fig. 1a, b were predicted by recent quantitative theories of spin propagation in a 2DEG in the presence of spin–orbit coupling. The effects on spin propagation of the Rashba interaction term in the Hamiltonian, $H_R = \alpha\hbar v_F(k_y\sigma_x - k_x\sigma_y)$, where v_F is the Fermi velocity, $\hbar\mathbf{k} \equiv \hbar(k_x, k_y, k_z)$ is the electron momentum ($\hbar$ denoting Planck's constant divided by 2π) and σ_x and σ_y are Pauli matrices, were studied in refs 11, 12. The term H_R corresponds to an in-plane, $\mathbf{k}$-dependent magnetic field, $\mathbf{b}_R = \alpha\hbar v_F(k_y\hat{\mathbf{x}} - k_x\hat{\mathbf{y}})$, that leads to precession of the electron's spin. It was found that, in the presence of $\mathbf{b}_R$, the normal modes of the system are helical waves of spin polarization in which the spin direction rotates in the plane normal to the 2DEG and parallel to the wavevector, $\mathbf{q}$ (Fig. 1c). For each $\mathbf{q}$, there are two helical modes with opposite senses of rotation. The lifetime of the mode whose sense of rotation matches the precession of the electron's spin is enhanced, and the lifetime of the other is reduced. A striking prediction is that, for a range of $\mathbf{q}$ values, the spin–orbit-enhanced lifetime will exceed that of a uniform ($q = 0$) spin polarization. This contrasts with ordinary diffusion, in which the decay rate for spin excitations scales as q^2 and the spin lifetime is always greatest at $q = 0$. (The same conclusions are reached when the linear Dresselhaus term, $H_D = \beta_1\hbar v_F(k_x\sigma_x - k_y\sigma_y)$, is assumed to be the only spin–orbit interaction). Experimental support for these predictions was reported[13], in which a maximum spin lifetime at non-zero q was observed in nominally symmetric GaAs quantum wells, where H_D dominates the spin–orbit Hamiltonian.

Recently, this theory has been extended to predict the lifetimes of helix modes in the presence of both H_R and H_D (ref. 2). In particular, it was predicted that as the two couplings approach equal strength, the spin–orbit-enhanced mode evolves to the PSH; that is, the lifetime tends to infinity for $\mathbf{q} = \mathbf{q}_{PSH}$. As discussed above, the stability of the PSH is a manifestation of SU(2) symmetry at this point in parameter space. Although conservation of the x' component (Fig. 1c) of spin, or U(1) symmetry, was noted previously[14], SU(2) symmetry implies conservation of the amplitude and phase of the PSH as well. The theory also predicts quantitatively how the persistence of the helix degrades with detuning from the SU(2) point, by variation either of $\mathbf{q}$ or the α/β_1 ratio. The theory has been extended further[15] by the inclusion of the SU(2)-breaking effects of the cubic Dresselhaus coupling

$$H_{cD} = -4\beta_3\frac{\hbar v_F}{k_F^2}(k_x k_y^2\sigma_x - k_y k_x^2\sigma_y)$$

(k_F is the Fermi wavevector) which is always present at some level because of the non-zero width of the quantum well (see below).

The predictions of helical spin modes described above are clearly evident in the TSG results shown in Fig. 1. The initial condition created by the two pump pulses—a sinusoidal of variation S_z at $t = 0$—is equivalent to two equal-amplitude S_y–S_z helices of opposite pitch. Each of these normal modes then decays independently with its own characteristic decay rate, corresponding to the spin–orbit-enhanced and -reduced helix lifetimes (τ_E and τ_R, respectively). The reduced lifetimes shown in Fig. 1b peak at $q = 0$, whereas the enhanced lifetime is greatest at a finite value of $\mathbf{q}$. The solid lines are a fit to the theory of ref. 15 using a single set of spin–orbit parameters for both the enhanced and reduced helix modes.

The fact that the dispersion of both branches is accurately fitted by a single set of spin–orbit parameters suggests that spin helices are indeed the normal modes of our spin–orbit-coupled 2DEGs. The theoretical fits provide us with values for α, β_1, β_3 and D_S (the spin-diffusion coefficient), which we then use to guide us in engineering quantum wells with the longest spin-helix lifetimes. To tune the spin–orbit Hamiltonian, we have designed a series of quantum-well samples with varying doping asymmetries and well widths.

Figure 2 summarizes the spin–orbit tuning results. To tune the Rashba interaction, which arises from asymmetry in the electron's confinement potential, we varied the relative concentration of remote dopants on the two sides of the 2DEG (keeping the total dopant concentration fixed). These measurements were performed at $T = 75$ K, at which temperature the enhanced-mode lifetimes are greatest (see discussion of T dependence below). The enhanced spin lifetimes, τ_E, are plotted as functions of q in Fig. 2a, for a set of 12-nm-wide quantum wells with varying amounts of doping asymmetry. The maximum lifetime and the wavevector at which it occurs grow monotonically with increasing dopant asymmetry. Figure 2b shows the spin–orbit parameters extracted from comparison of the dispersion curves with the theory of ref. 15, for each of the samples. The parameters α, β_1 and β_3 are plotted as functions of normalized asymmetry, defined as the difference between the concentrations of dopant ions on either side of the well, divided by the total dopant concentration. The variation in α is well approximated by a straight line that extrapolates to zero coupling as the asymmetry parameter goes to zero. The data for the nominally symmetric sample display a residual Rashba coupling, which we attribute to the inherent asymmetry in the growth of the quantum wells[13,16–18]. Although only τ_E is shown in Fig. 2a, the high decay rates are accurately described by the same set of parameters.

The linear Dresselhaus interaction is related to the degree of confinement of the electrons (that is, it is proportional to $\langle k_z^2\rangle$). We tune the linear Dresselhaus interaction by varying the width, d, of each quantum well, with the normalized asymmetry fixed at unity. Experimentally determined spin lifetimes and theoretical fits are plotted in Fig. 2c for values of d ranging from 7 to 15 nm. The peak value of τ_E shows a clear maximum, suggesting that as d is varied the spin–orbit Hamiltonian approaches and then recedes from the SU(2) point. The curves generated from the theory of ref. 15 fit the data very

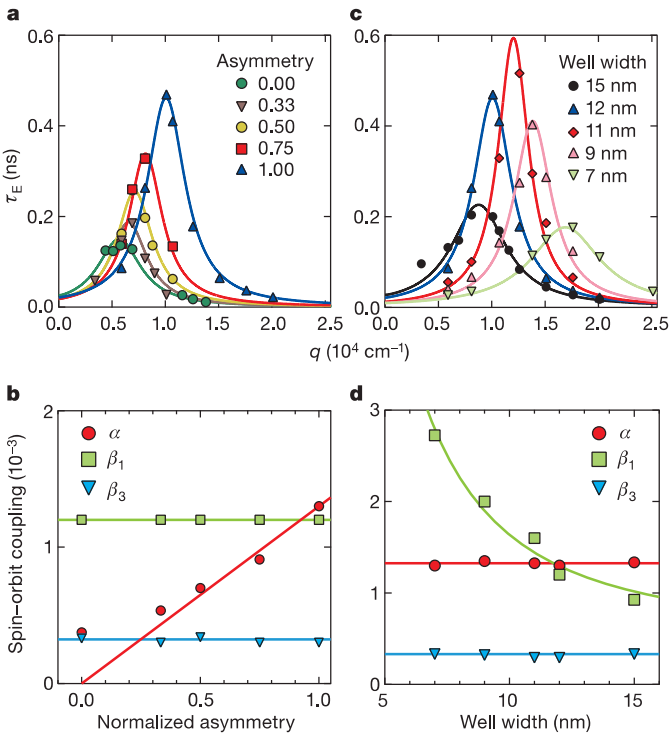

Figure 2 | Rashba and linear Dresselhaus tuning. **a**, **c**, Lifetimes of the enhanced helix mode are shown for samples with varying degrees of doping asymmetry (**a**) and well width (**c**). The normalized asymmetry is the difference between the concentrations of dopants on either side of the well, divided by the total dopant concentration. The solid lines are fits to the theory of ref. 15 (see text). **b**, **d**, Plots summarizing the spin–orbit parameters from these fits in **a** and **c**. As in ref. 15, the spin–orbit coupling strengths are expressed as dimensionless quantities by normalizing to the Fermi velocity.

well, with both α and β_3 remaining essentially constant, indicating that we have varied β_1 independently. The spin–orbit parameters for each sample in the series are plotted in Fig. 2d. The crossing of α and β_1 occurs at a well width near 12 nm; however, the largest τ_E value occurs in the 11-nm sample. This finding is consistent with theory[15], which predicts that for constant D_S the peak lifetime occurs for $\alpha = \beta_1 - \beta_3$ rather than for $\alpha = \beta_1$. (When τ_E is normalized to account for variations in D_S from one sample to another, the same condition holds for asymmetry series as well; see Supplementary Information.)

As a check on the modelling of our TSG data, we compare the experimental values of α, β_1 and β_3 with band structure calculations. The Rashba coupling strength is predicted to obey $\alpha = r_{41}^{6c6c} e\langle E_z\rangle/\hbar v_F$, where e is the elementary charge, $\langle E_z\rangle$ is the average electric field in the well and r_{41}^{6c6c} is an intrinsic proportionality factor. In **k**·**p** perturbation theory, this factor is found to be 5.206 Å^2 for GaAs (ref. 19). To make a comparison with theory, we assume that the electrons in the well experience the delta layers as an infinite sheet of positive charge. We estimate the field strength to be 5.4×10^6 V m^{-1} for a normalized asymmetry of one. From the corresponding value of α, we find that $r_{41}^{6c6c} = 6.7$ Å^2, in good agreement with the perturbation theory result.

The Dresselhaus couplings, β_1 and β_3, are both proportional to a single intrinsic parameter, γ, with the linear term given by $\beta_1 = \gamma\langle k_z^2\rangle k_F/2E_F$, where E_F is the Fermi energy. From the values of β_1 as a function of well width, determined by TSG spectroscopy and analysis using the theory of ref. 15, we estimate that $\gamma = 5.0$ eV Å^3, assuming that $\langle k_z^2\rangle = (\pi/d)^2$. A larger value of γ would be obtained if $\langle k_z^2\rangle$ were reduced by penetration of the electron wavefunction into the barrier. Theoretical calculation of γ has proven to be challenging, and a wide range of values, 6.5–30 eV Å^3, have been reported for bulk GaAs (refs 20, 21). Comparison with experiment is further complicated by the existence of an interface Dresselhaus term, which, although often neglected, may be important in two-dimensional structures such as those studied here[22]. In the light of these complications, the value of γ that we obtain is in reasonable agreement with theory. It is also important to note that the experiments reported here potentially offer heightened sensitivity to the cubic Dresselhaus interaction, as proximity to the SU(2) point effectively eliminates spin relaxation from the linear terms. Independent of the value of γ, the ratio β_3/β_1 is given theoretically by $k_F^2/4\langle k_z^2\rangle$; that is, it is proportional to the ratio of the electron kinetic energies respectively parallel and perpendicular to the conducting plane. Again estimating that $k_z = \pi/d$, we find that the expected ratio for an 11-nm well is 0.16, consistent with our experimental value of 0.2. This agreement between theory and experiment supports the notion that the cubic Dresselhaus interaction limits the PSH lifetime in our samples at low temperature.

The T dependence of the spin-helix lifetimes further tests our understanding of 2DEG spin physics, and also is relevant to potential spintronics applications. The T dependence of the lifetime of each mode, for the sample closest to the SU(2) point, is plotted on a logarithmic scale in Fig. 3a. The lifetime of the spin–orbit-enhanced mode increases with decreasing T to ~50 K, then drops rapidly with further lowering of T. The lifetime of the spin–orbit-reduced mode, on the other hand, decreases monotonically with decreasing T.

We cannot rely solely on the spin dynamics theories described previously to explain the observed T dependence, as they consider only the $T = 0$ limit. However, these theories do indicate an important first step in the analysis. For a given set of spin–orbit parameters, the spin-helix lifetimes for both senses of rotation, and for all q, are predicted to scale as D_S^{-1}. Because D_S is known to depend strongly on T (ref. 23), this scaling provides at least one well-understood mechanism for T-dependent lifetimes. However, the fact that the enhanced- and reduced-lifetime modes display very different temperature dependences indicates immediately that scaling by $D_S(T)$ cannot fully account for the effect of temperature.

To focus on the T-dependent effects other than scaling by D_S, we consider the dimensionless parameter $\eta \equiv D_S q_{PSH}^2 \tau_{PSH}$, rather than

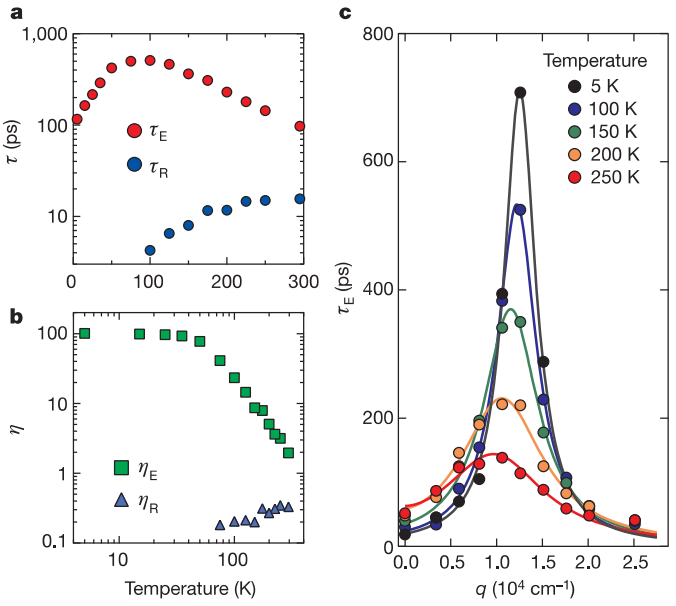

Figure 3 | Temperature dependence of the PSH. a, Temperature dependence of the lifetime of each helix mode at q_{PSH} for the 11-nm, asymmetrically doped sample, which is the closest to the SU(2) point. **b**, Temperature dependence of the dimensionless lifetime-enhancement factor $\eta \equiv D_S q_{PSH}^2 \tau_{PSH}$ for each helix mode. **c**, Temperature dependence of the PSH dispersion curves for a similar sample with a slightly reduced mobility. The reduced mobility suppresses the drop in D_S and τ by avoiding the ballistic crossover. Fits to the theory of ref. 15 (solid lines) are also shown.

τ_{PSH} itself (here the subscript PSH refers to quantities evaluated at the PSH wavevector). The parameter η is the measured PSH lifetime normalized to the lifetime predicted in the absence of spin–orbit coupling (see Methods), that is, a direct measure of the lifetime enhancement as a result of proximity to the SU(2) point. Figure 3b is a logarithmic plot of $\eta(T)$ for both helix modes. The enhancement factor corresponding to the rapidly decaying mode, η_R, is essentially independent of T, indicating that the temperature dependence of τ_R is entirely accounted for by $D_S(T)$. (The rapid increase of D_S below 75 K is the result of the quenching of the spin-Coulomb-drag effect[23,24].) By contrast, η_E is strongly T dependent. In this case, normalization with respect to $D_S(T)$ converts the peak in τ_E near 75 K to a plateau at low values of T, demonstrating that the PSH-lifetime enhancement is a monotonically decreasing function of increasing T. The enhancement factor is approximately 100 at low values of T and decays towards unity (no spin–orbit enhancement) at high temperature. Above 50 K, the enhancement factor obeys the power law $\eta(T) \propto T^{-2.2}$. In Fig. 3c, we plot the spin-lifetime dispersion curves for several values of T, illustrating the damping of the entire PSH resonance with increasing temperature. Although weakened, the PSH remains observable at room temperature. The existence of the PSH at temperatures far greater than that equivalent to the spin–orbit spin-splitting energy, which is only ~1 K, supports the idea that the lifetime enhancement is symmetry driven.

Why the PSH stability decreases strongly with T remains an open question. Within a non-interacting (or single-particle) picture, the cubic Dresselhaus term is the only SU(2)-breaking interaction. In the two-dimensional limit, where $\beta_3 = \beta_1$, the cubic Dresselhaus term can be viewed as a small, velocity-dependent correction to β_1, that is, $\beta_1^{eff} = \beta_1 - \beta_3 v^2/v_F^2$ (ref. 25). With increasing T, the thermal average of β_1^{eff} will decrease, driving the effective spin–orbit Hamiltonian farther from the SU(2) point. However, it is not clear at present whether this effect is sufficiently strong to account for the T dependence depicted in Fig. 3. A relatively weak reduction in PSH stability with increasing T was observed in numerical simulations of the spin kinetic equations for the specific case of $\alpha = 0.3\beta_1$ (ref. 25), and simulations with $\alpha \approx \beta_1$

have not yet been reported. To estimate the T dependence expected in this regime, we can substitute the thermal average of β_1^{eff} for β_1 in the formulae of ref. 15 for the PSH lifetime. Although we do obtain $\eta(T) \propto T^{-2}$ in the high-temperature limit, the onset of T^{-2} dependence is at approximately the Fermi temperature, which is ~400 K for our quantum wells. As the measured onset of the $T^{-2.2}$ dependence is at roughly 50 K, the nonlinear velocity dependence of β_1^{eff} may not fully account for the reduction in PSH lifetime with temperature. In considering effects beyond the single-particle picture, the approximate T^{-2} scaling suggests a connection with electron–electron scattering. As mentioned previously, if SU(2) symmetry is exact then the PSH lifetime is not sensitive to electron–electron scattering[2]. However, it remains to be seen whether many-body interactions can affect the PSH lifetime when SU(2) is weakly broken by the cubic Dresselhaus term, disorder in local spin–orbit couplings[26] or spin-dependent scattering mechanisms.

Finally, we note that a PSH-lifetime enhancement of 100 is not a fundamental limit. When controlled by the cubic Dresselhaus term, the lifetime enhancement is proportional to $(\beta_1/\beta_3)^2$. Gated structures in which electron density and electric field are tuned independently will enable this ratio to be increased, while maintaining $\alpha = \beta_1$. Increased stability of the PSH creates possibilities for new experiments on spin transport, such as the measurement of the intrinsic spin Hall effect, the study of charge transport dynamics in the presence of strong spatial variation of spin polarization and the demonstration of efficient spin transistors.

METHODS SUMMARY

The GaAs/$Al_{0.3}Ga_{0.7}$As quantum-well samples were grown on semi-insulating GaAs in the [001] direction by molecular beam epitaxy, and consisted of ten quantum wells separated by 48-nm barriers. The Si donors were deposited in eight single-atomic layers in the central 14 nm of each barrier to maximize their distance from the 2DEG. To tune α, the ratio of the donor concentrations in alternating barriers was adjusted by varying the Si deposition times, and the total target carrier concentration in the wells was held fixed at $n = 8 \times 10^{11}\,\mathrm{cm}^{-2}$. The electron mobility typically reached $\mu \approx 3 \times 10^5\,\mathrm{cm}^2\,\mathrm{V}^{-1}\,\mathrm{s}^{-1}$ at low temperature. All samples were mounted on c-axis-cut sapphire discs, and the GaAs substrates were chemically etched to allow for spin-grating measurements in transmission geometry.

We determined the spin diffusion coefficient, D_S, through analysis of the uniform spin polarization, $S_z(q = 0, t)$, measured by a standard time-resolved Faraday rotation technique[10]. As T was reduced from room temperature, $S_z(q = 0, t)$ crossed over from single-exponential decay to damped oscillations (at about 50 K in our quantum wells). The crossover occurred when the electron mean free time became comparable to the period of precession in the spin–orbit effective fields. In the high-T regime, we determined D_S from $1/\tau_S = D_S q_{\mathrm{PSH}}^2$ (ref. 27), which holds in the regime where α and β_1 are approximately equal. Here τ_S is the $q = 0$ spin lifetime. To determine D_S through the crossover regime, we used the phenomenological formula

$$S_z(q=0,\,t) \propto \int_0^{\pi/2} \exp\left(-\frac{\Omega\tau\cos\phi}{1-i\Omega\tau\cos\phi}\,\Omega t\right) \mathrm{d}\phi$$

where τ is the mean free time and $\Omega\cos\phi$ is the precession frequency as function of angle, ϕ, on the Fermi circle. This expression interpolates between the exact result in the $\Omega\tau \gg 1$ limit, which is the zero-order Bessel function, and the non-oscillatory decay in the $\Omega\tau \ll 0$ limit. We verified that the values of D_S obtained from the $q = 0$ data are consistent with those obtained from analysis of the full q dependence of the spin lifetimes.

Full Methods and any associated references are available in the online version of the paper at www.nature.com/nature.

Received 10 October 2008; accepted 30 January 2009.

1. Noether, E. Invariante Variationsprobleme. Nachr. König. Gesellsch. Wiss. Göttingen, Math-Phys. Klasse 235–257 (1918).
2. Bernevig, B. A., Orenstein, J. & Zhang, S.-C. Exact SU(2) symmetry and persistent spin helix in a spin-orbit coupled system. Phys. Rev. Lett. 97, 236601 (2006).
3. Bychkov, Y. A. & Rashba, E. I. Oscillatory effects and the magnetic susceptibility of carriers in inversion layers. J. Phys. Chem. 17, 6039–6045 (1984).
4. Dresselhaus, G. Spin–orbit coupling effects in zinc blende structures. Phys. Rev. 100, 580–586 (1955).
5. Cameron, A. R., Riblet, P. & Miller, A. Spin gratings and the measurement of electron drift mobility in multiple quantum well semiconductors. Phys. Rev. Lett. 76, 4793–4796 (1996).
6. Awschalom, D. D., Loss, D. & Samarth, N. (eds) Semiconductor Spintronics and Quantum Computation (Springer, 2002).
7. Ohno, M. & Yoh, K. Datta-Das-type spin-field-effect transistor in the nonballistic regime. Phys. Rev. B 77, 045323 (2008).
8. Meier, F. & Zakharchenya, B. Optical Orientation (North-Holland, 1984).
9. Gedik, N. & Orenstein, J. Absolute phase measurement in heterodyne detection of transient gratings. Opt. Lett. 29, 2109–2111 (2004).
10. Crooker, S. A., Awschalom, D. D. & Samarth, N. Time-resolved Faraday rotation spectroscopy of spin dynamics in digital magnetic heterostructures. IEEE J. Sel. Top. Quantum Electron. 1, 1082–1092 (1995).
11. Froltsov, V. A. Diffusion of inhomogeneous spin distribution in a magnetic field parallel to interfaces of a III–V semiconductor quantum well. Phys. Rev. B 64, 045311 (2001).
12. Burkov, A. A., Nunez, A. S. & MacDonald, A. H. Theory of spin-charge-coupled transport in a two-dimensional electron gas with Rashba spin-orbit interactions. Phys. Rev. B 70, 155308 (2004).
13. Weber, C. P. et al. Nondiffusive spin dynamics in a two-dimensional electron gas. Phys. Rev. Lett. 98, 076604 (2007).
14. Schliemann, J., Egues, J. C. & Loss, D. Nonballistic spin-field-effect transistor. Phys. Rev. Lett. 90, 146801 (2003).
15. Stanescu, T. D. & Galitski, V. Spin relaxation in a generic two-dimensional spin-orbit coupled system. Phys. Rev. B 75, 125307 (2007).
16. Braun, W. Trampert, A. Däweritz, L. & Ploog, K. H. Nonuniform segregation of Ga at AlAs/GaAs heterointerfaces. Phys. Rev. B 55, 1689–1695 (1997).
17. de Andrada e Silva, E. A. La Rocca, G. C. & Bassani, F. Spin-orbit splitting of electronic states in semiconductor asymmetric quantum wells. Phys. Rev. B 55, 16293–16299 (1997).
18. Schubert, E. F. et al. Fermi-level-pinning-induced impurity redistribution in semiconductors during epitaxial growth. Phys. Rev. B 42, 1364–1368 (1990).
19. Winkler, R. Spin–Orbit Coupling Effects in Two-Dimensional Electron and Hole Systems (Springer Tracts Mod. Phys. Vol. 191, Springer, 2003).
20. Krich, J. J. & Halperin, B. I. Cubic Dresselhaus spin-orbit coupling in 2D electron quantum dots. Phys. Rev. Lett. 98, 226802 (2007).
21. Chantis, A. N., Schilfgaarde, M. & Kotani, T. Ab initio prediction of conduction band spin splitting in zinc blende semiconductors. Phys. Rev. Lett. 96, 086405 (2006).
22. Fabian, J., Matos-Abiague, A., Ertler, C., Stano, P. & Zutic, I. Semiconductor spintronics. Acta Physica Slovaca 57, 565–907 (2007).
23. D'Amico, I. & Vignale, G. Spin Coulomb drag in the two-dimensional electron liquid. Phys. Rev. B 68, 045307 (2003).
24. Weber, C. P. et al. Observation of spin Coulomb drag in a two-dimensional electron gas. Nature 437, 1330–1333 (2005).
25. Weng, M. Q., Wu, M. W. & Cui, H. L. Spin relaxation in n-type GaAs quantum wells with transient spin grating. J. Appl. Phys. 103, 063714 (2008).
26. Sherman, E. & Ya.. Random spin–orbit coupling and spin relaxation in symmetric quantum wells. Appl. Phys. Lett. 82, 209–211 (2003).
27. D'Yakonov, M. I., &. Perel', V. I. Spin relaxation of conduction electrons in noncentrosymmetric semiconductors. Sov. Phys. Solid State 13, 3023–3026 (1971).

Supplementary Information is linked to the online version of the paper at www.nature.com/nature.

Acknowledgements Work performed at Lawrence Berkeley National Laboratory and Stanford University was supported by the US Department of Energy, Office of Basic Energy Science, Materials Science and Engineering Division, and at the University of California, Santa Barbara by the US National Science Foundation and Office of Naval Research. S.M. acknowledges partial support through the National Defense Science and Engineering Graduate Fellowship Program. We thank J. Stephens and J. Krich for discussions, G. Fleming for use of a phase-mask array, and K. Bruns for creating the PSH diagram of Fig. 1c.

Author Information Reprints and permissions information is available at www.nature.com/reprints. Correspondence and requests for materials should be addressed to J.D.K. (jdkoralek@lbl.gov).

METHODS

Transient spin gratings. Transient spin polarization waves were generated by the optical interference of two cross-polarized pulses from a single mode-locked Ti:sapphire laser (80 MHz, 100 fs), focused non-collinearly onto the 2DEG. The pump pulses were amplitude-modulated at 100 kHz using a photo-elastic modulator. The time evolution of the spin polarization was monitored by time-delayed probe pulses, which see the modulation of the 2DEG polarization as a diffraction grating because of the Kerr effect. The amplitude and phase of the transient spin grating were measured using a heterodyne detection scheme. The diffracted pulses were mixed at a Si photodiode detector with another beam from the same laser, which served as a local oscillator[9]. The relative phase of the signal and local oscillator pulses was modulated at 210 Hz by transmitting one beam through a coverslip mounted on a torsional oscillator. Synchronous detection of the mixed signal was accomplished using two lock-in amplifiers, the first referenced to the pump amplitude-modulation frequency and the second referenced to the modulation frequency of the relative phase.